

Superconductivity in graphite intercalation compounds with sodium

Chun-Mei Hao^{1,2}, Xing Li², Artem R. Oganov³, Jingyu Hou⁴, Shicong Ding², Yanfeng Ge², Lin Wang^{1,2},
Xiao Dong⁴, Hui-Tian Wang⁵, Guochun Yang^{2,*}, Xiang-Feng Zhou^{1,2,*}, and Yongjun Tian¹

¹*Center for High Pressure Science, State Key Laboratory of Metastable Materials Science and Technology, Yanshan University, Qinhuangdao, 066004, China*

²*Key Laboratory for Microstructural Material Physics of Hebei Province, School of Science, Yanshan University, Qinhuangdao 066004, China*

³*Skolkovo Institute of Science and Technology, Bolshoy Boulevard 30, bld. 1, Moscow 121205, Russia*

⁴*Key Laboratory of Weak-Light Nonlinear Photonics, School of Physics, Nankai University, Tianjin 300071, China*

⁵*National Laboratory of Solid State Microstructures, School of Physics, and Collaborative Innovation Center of Advanced Microstructures, Nanjing University, Nanjing 210093, China*

Email: yanggc@ysu.edu.cn; xfzhou@ysu.edu.cn

The discovery of superconductivity in CaC_6 with a critical temperature (T_c) of 11.5 K reignites much interest in exploring high-temperature superconductivity in graphite intercalation compounds (GICs). Here we identify a GIC NaC_4 , discovered by *ab initio* evolutionary structure search, as a superconductor with a computed T_c of 41.2 K at 5 GPa. This value is eight times higher than that of the synthesized GIC NaC_2 and possesses the highest T_c among available GICs. The remarkable superconductivity of GIC NaC_4 mainly arises from the coupling of π electrons in graphene with the low-frequency vibrations involving both Na and C atoms. These findings suggest that Na-GIC may hold great promise as a high- T_c superconductor.

I. Introduction

The search for high-temperature superconductors and the discovery of their origins are ongoing topics in condensed matter physics [1-3]. Bardeen-Cooper-Schrieffer (BCS) theory allows one to calculate properties of conventional superconductors. Compounds made of light elements usually have a high Debye temperature, which favors high-temperature superconductivity [4,5]. Thus far, pressurized hydrides, the most promising candidate, have demonstrated remarkably high critical temperatures (T_c s) that approach room temperature [6,7]. However, maintaining their superconductivity requires extremely high pressure of \sim 150 GPa or more [8,9], which presents strict requirements for scientific instruments and precludes practical applications. In this regard, the discovery of high- T_c superconductors stabilized at low pressure or even at ambient pressure is the next recognized target [10,11].

Carbon is the sixth element in the periodic table and has a low atomic mass. Carbon forms the richest variety of allotropes and compounds among the light elements due to diverse hybridizations (e.g., sp , sp^2 , and sp^3) [12-14]. An intriguing feature is that some carbon-based materials synthesized at high temperatures and high pressures can be quenchable to ambient conditions. Therefore, the investigation of superconductivity in carbon-based materials has always been in focus, and new discoveries continue to emerge [15-19]. For instance, multiple types of carbon-based superconductors have been confirmed, including B doped diamond, Q-carbon, graphite-diamond hybrid (3D carbon framework) [16-19], YbC_6 and CaC_6 (GICs, 2D carbon framework) [20,21], Li_2C_2 (1D carbon form) [22], and alkali metal doped C_{60} (0D carbon form) [23,24].

GICs are typical layered compounds formed by inserting other atoms or molecules into interlayer spaces of graphite. The species of intercalants and their stoichiometries can modify the stacking pattern, arrangement of intercalated atoms, and the interlayer spacing. Generally, an n -stage GIC represents n successive graphene layers that are separated by the intercalant species [25]. It is evident that pressure can modify the metal concentration in GICs [26]. These features make GICs with the rich structures and intriguing properties, especially for superconductivity which is absent in graphite. Among the reported superconducting GICs, CaC_6 has the highest T_c of 11.5 K at ambient pressure, and this increases further to 15.1 K at 7.5 GPa [20,21,27]. Since then, no other GICs could break this T_c record. Unlike alkali metals of Li and K, Na does not form GIC at ambient conditions and this is why GICs NaC_2 and NaC_3 have been synthesized at pressures ranging from 1.6 to 3.7 GPa [28,29]. In particular, GIC NaC_2 exhibits a measured T_c of 5.0 K at 3.5 GPa, but its crystal structure remains unresolved. Meanwhile, it is unknown whether there are other Na-GICs under pressure and whether they are superconducting. With these points in mind, we systematically explored various chemical compositions of potential Na-C compounds at pressures of 5 and 10 GPa, focusing on GICs that have not been previously investigated [30].

II. Computational Methodology

Crystal structure prediction has played a major role in accelerating the discovery of new materials, especially at extreme conditions [31-36]. In this work, the variable-composition evolutionary algorithm USPEX was utilized to predict thermodynamically stable compounds in the Na-C system [31,32]. At the selected pressures, structure searches were conducted with an

unbiased sampling of the entire range of compositions, simultaneously varying the stoichiometries and the corresponding structures. Structure relaxations and electronic properties calculations were carried out within the framework of density functional theory [37,38] as implemented by the Vienna *ab initio* simulation package (VASP) [39]. The generalized gradient approximation (GGA) of Perdew-Burke-Ernzerhof (PBE) functional was employed for the calculation [40]. The projector augmented wave (PAW) pseudopotentials [41], with $2s^22p^63s^1$ and $2s^22p^2$ valence electrons for Na and C atoms, were used to describe the interactions between electrons and ions. A plane wave basis set with a cutoff of 1000 eV and the k -point meshes with a resolution better than $2\pi \times 0.022 \text{ \AA}^{-1}$ in the reciprocal space were used to ensure the total energy convergence (10^{-6} eV/cell). We fully relaxed the lattice parameters and atomic coordinates until the force on each atom was less than 0.001 eV/ \AA .

The Quantum ESPRESSO package [42] was used to calculate lattice dynamics and electron-phonon coupling (EPC) using Norm-conserving pseudopotentials. The wave function cutoff energy was 150 Ry, and the charge density cutoff energy was 600 Ry. Different k -mesh (q -mesh) were chosen for the predicted compounds: $15 \times 15 \times 9$ ($5 \times 5 \times 3$) for $P2_1/m$ NaC_2 , $12 \times 12 \times 12$ ($6 \times 6 \times 6$) for $Cmcm$ NaC_4 and $16 \times 16 \times 16$ ($8 \times 8 \times 8$) $P6/mmm$ NaC_6 . In addition, EPC calculations were also performed for GIC CaC_6 with ultrasoft pseudopotentials. The cutoff energy of wave functions and the q -mesh are adopted using 55 Ry and $4 \times 4 \times 4$, respectively [43]. The T_c value was estimated by the Allen-Dynes-modified McMillan formula [44],

$$T_c = \frac{\omega_{\log}}{1.2} \exp\left[-\frac{1.04(1+\lambda)}{\lambda - \mu^*(1+0.62\lambda)}\right],$$

where λ is the EPC strength, ω_{\log} is the logarithmic average phonon frequency, and μ^* is the Coulomb pseudopotential parameter. The parameters λ and ω_{\log} are defined as

$$\lambda = 2 \int_0^\infty \frac{\alpha^2 F(\omega)}{\omega} d\omega,$$

and

$$\omega_{\log} = \exp\left[\frac{2}{\lambda} \int_0^\infty \frac{d\omega}{\omega} \alpha^2 F(\omega) \ln \omega\right],$$

respectively.

III. Result and Discussion

The enthalpy of formation (ΔH_f) is defined as $\Delta H_f(\text{Na}_x\text{C}_{1-x}) = H(\text{Na}_x\text{C}_{1-x}) - xH(\text{Na}) - (1-x)H(\text{C})$, where H represents the enthalpy of compounds or elemental solids. At a given pressure, the Na-C structures located

on the convex hulls (indicated by solid lines in Fig. 1a) are thermodynamically stable against decomposition into other binary compounds and elemental solids. As illustrated in Fig. 1a, NaC_2 with $P2_1/m$ symmetry and NaC_6 with $P6/mmm$ symmetry are thermodynamically stable at 5 GPa, which is partially consistent with the experimental results where the first-stage GIC NaC_2 and NaC_3 were synthesized below 4 GPa. At 10 GPa, NaC_4 with $Cmcm$ symmetry emerges on the convex hull, but NaC_6 is metastable. To provide more information for potential experimental study, the pressure-composition phase diagram was plotted in Fig. 1b, which demonstrates the thermodynamic stability range of the predicted compounds. Specifically, $P2_1/m$ NaC_2 is stable in the pressure range from 4.4 to at least 10 GPa, and from 2.9 to 9.3 GPa for $P6/mmm$ NaC_6 , whereas $Cmcm$ NaC_4 is stable above 8.9 GPa. The pressure of formation for Na-GICs should be easily accessible within the current experimental technology, i.e., large-volume multi-anvil system or diamond anvil cell experiments. What is more important, these predicted high-pressure structures may be quenchable to ambient pressure (Figs. S1(a)-(c)) [45], giving them potential practical value.

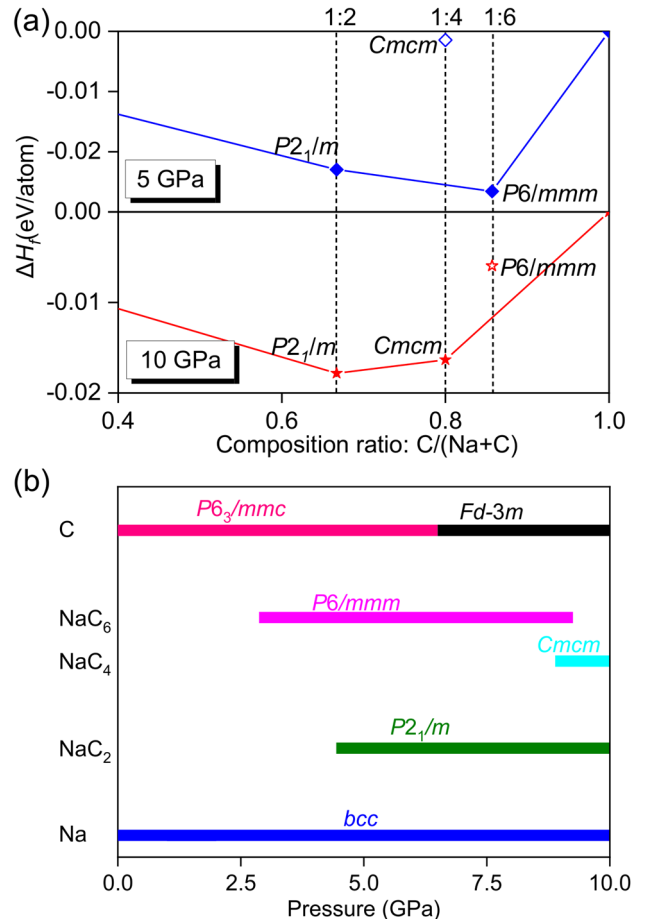


Fig. 1. (a) The calculated convex hulls for the Na-C systems at 5 and 10 GPa. The elemental reference structures are *bcc*-Na, graphite at 5 GPa, and diamond at 10 GPa, respectively. (b)

Pressure-composition phase diagram of Na-C compounds within the pressure range from 0 to 10 GPa.

As shown in [Fig. 2](#), the three compounds demonstrate a common structural feature: the C atoms constitute the honeycomb-like graphene, and the Na atoms are located within the voids of the graphene interlayers. As a result, all of the predicted stable phases belong to the first-stage GICs. Their lattice parameters and atomic positions at 5 GPa are listed in [Table S1](#) [45]. $P2_1/m$ NaC₂ has a monoclinic structure, in which the Na atoms form double layers with the nearest distance ~ 3.28 Å. Two adjacent Na layers are interconnected by zigzag chain with a distance ~ 3.32 Å ([Fig. 2a](#)). $Cmcm$ NaC₄ stabilizes into an orthorhombic structure ([Fig. 2b](#)) above 8.9 GPa, where the Na atoms are arranged in a zigzag-like configuration with the nearest distance ~ 3.12 Å ([Fig. 2b](#)). Notably, metal atoms in GICs usually locate above the center of hexagonal carbon ring, but Na atoms in NaC₄ significantly deviate from the center. Here, we have constructed a hypothetical model of c -NaC₄ by moving the Na atoms above the center of hexagonal carbon ring. After structure relaxation, Na atoms in c -NaC₄ return to the original positions of $Cmcm$ NaC₄. In other words, Na atoms in $Cmcm$ NaC₄ prefer to locate above the off-center configuration. $P6/mmm$ NaC₆ has Na atoms arranged in a triangular form with the nearest distance of ~ 4.31 Å ([Fig. 2c](#)), similar to the B layer in $P6/mmm$ BH [46]. Moreover, the stacking sequence of graphene and Na layers in $P6/mmm$ NaC₆ is $A\alpha A\alpha$, which differs from that in $R-3m$ CaC₆, where it is $A\alpha A\beta A\gamma A$ [47]. The C-C bonding lengths in the Na-GICs are slightly larger than those in pristine graphene ([Table S2](#)) [45,48], which can be attributed to the charge transfer from Na to C, leading to the electronic occupation of C-C antibonding orbital, weakening the covalent C-C bonds ([Figs. S2\(a\)-\(c\)](#)) [45].

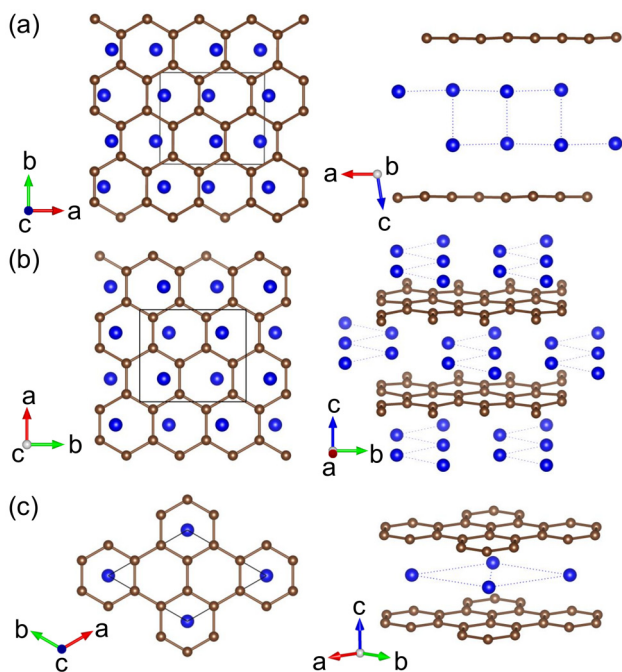


Fig. 2. Crystal structures of Na-GICs at 5 GPa. (a) $P2_1/m$ NaC₂, (b) $Cmcm$ NaC₄, and (c) $P6/mmm$ NaC₆. For these structures, the blue and brown spheres represent Na and C atoms, respectively.

Inspired by the unique structures of the three predicted Na-GICs, we proceeded to explore their electronic properties through calculating projected electronic band structures and density of states (DOS). The three phases demonstrate intrinsic metallicity with several bands crossing the Fermi level (E_F , see [Fig. 3a](#) and [Fig. S3\(a\)-\(d\)](#)) [45]. The normalized electronic DOS at E_F are ~ 0.02 states/(eV·Å³) for NaC₂ and NaC₆ at 5 GPa, whereas ~ 0.024 states/(eV·Å³) for NaC₄. Among three Na-GICs, the Fermi level of NaC₄ is closest to the Van Hove singularities ([Fig. 3b](#), [Figs. S3b](#) and [S3d](#)), implying that it may have better superconductivity [45]. Subsequently, we focused on analyzing the electronic properties of $Cmcm$ NaC₄. At 5 GPa, its metallicity mainly arises from the C p_z orbital electrons ([Fig. 3b](#)), which form a system of delocalized π bonds. The delocalized π electrons in the honeycomb-like graphene play a critical role in metallicity. One can notice steep bands along the S-R, R-Z, and Z-T directions and flat bands at the high symmetry points T and Γ near E_F ([Fig. 3b](#)), signifying the high electron velocity and large DOS.

The topology of the Fermi surface is helpful in understanding the behavior of electrons at E_F . For $Cmcm$ NaC₄, there are three bands crossing E_F ([Fig. 3c](#) and [Fig. S4](#)) [45]. Here, we explore band1 and band2, which make the dominant contribution to the Fermi surface. The Fermi surface of band1 consists of eight sheets, whereas band2 is composed of one “8”-type and two U-type sheets. Besides the minor contribution of Na p states to the Fermi surface from band2, the two Fermi surfaces are mainly derived from the C p_z states. More interestingly, the two Fermi surfaces are nested along the body diagonal and Γ -Z/S/Y direction of Brillouin zone (BZ). It is known that nesting can lead to a superconductivity or instability. It could be in favor of EPC since NaC₄ is mechanically and dynamically stable under pressure ([Fig. 3c](#)).

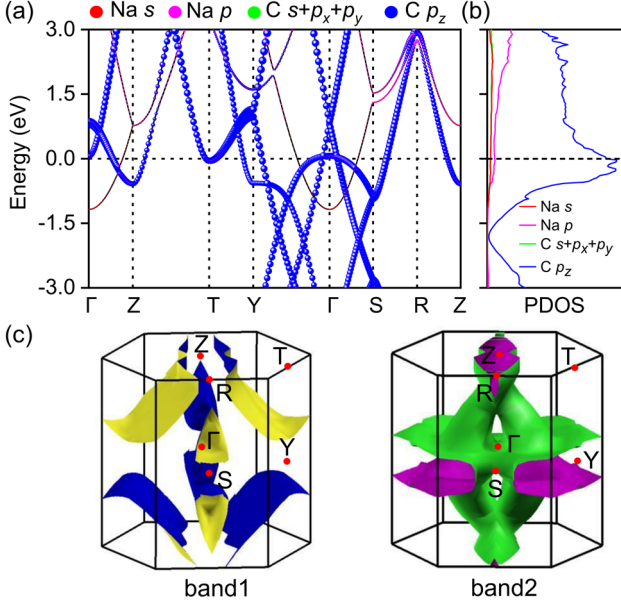


Fig. 3. (a) The orbital-resolved band structures of *Cmcm* NaC4 at 5 GPa. (b) Projected density of states (PDOS) (the dashed line indicates E_F). (c) The Fermi surfaces associated with two bands crossing E_F .

To establish the reliability of our computation method, we first employed the Allen-Dynes modified McMillan equation to estimate the superconductivity of GIC CaC₆. The calculated values of λ , ω_{\log} , and T_c are 0.78, 349.2 K and 11.4 K, respectively, with $\mu^* = 0.14$, which is in good agreement with both theoretical and experimental results [20,21,44,49]. For Na-GICs, superconductivity of *P2₁/m* NaC₂ at 3.5 GPa was also calculated with $\mu^* = 0.1$ (Fig. S6) [45]. The computed T_c of 5.4 K is in excellent agreement with the measured value of 5.0 K in NaC₂ at 3.5 GPa [28]. By contrast, the calculated EPC parameter λ of *Cmcm* NaC₄ is 1.01 at 5 GPa, comparable to MgB₂ (1.0 at 0 GPa) [50]. The phonon dispersion curves with λ weights show strong EPC in the range of 0-479 and 1200-1448 cm⁻¹ in the whole BZ (Fig. 4(a)), especially in the range of 0-479 cm⁻¹ along the Γ -Z, Γ -Y, and Γ -S directions. This result mostly related to phonon softening consistent with the Fermi surface nesting, supported by the distinct sharp peaks of the Fermi surface nesting function ξ_q (Fig. 4d). By comparing the Eliashberg spectral function $\alpha^2F(\omega)$ and PHDOS, we found that low frequency phonons (below 479 cm⁻¹), associated with Na and C coupling vibrations, contributes 70% to λ , while high-frequency phonons (479-1448 cm⁻¹) contribute 30% (Fig. 4(b)-4(c)). The latter is related to vibrations of strong covalent C-C bonds. As a result, superconductivity of NaC₄ predominantly originates from the coupling of C p_z electrons with the low-frequency phonons. The estimated T_c is 41.2 K at 5 GPa with a value of $\mu^* = 0.1$, making it the highest among the reported GICs [47]. The pressure-dependent superconductivity of NaC₄ at the pressures of 0, 5, and 10 GPa is also investigated (Fig. 4e). At zero pressure, the estimated T_c of *Cmcm*

NaC₄ is 36.6 K. With increasing pressure, T_c rises first (41.2 K at 5 GPa) and then falls (38.3 K at 10 GPa), which can be explained by the variations of ω_{\log} and λ . From 0 to 5 GPa, λ remains unchanged for *Cmcm* NaC₄, while ω_{\log} is significantly enhanced due to phonon stiffening, leading to a higher T_c value. As the pressure increases from 5 to 10 GPa, both ω_{\log} and λ gradually decrease, leading to the decline of T_c .

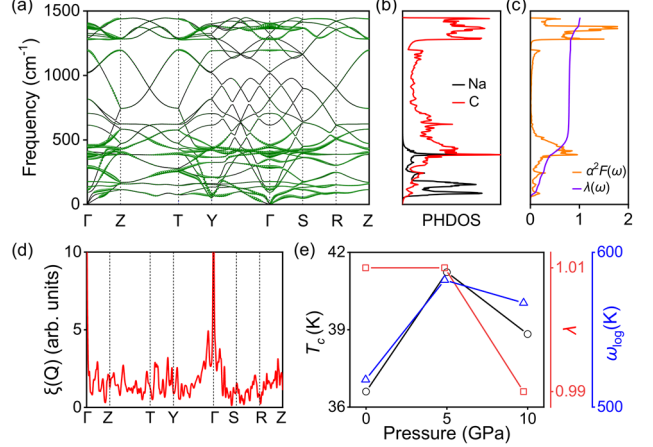


Fig. 4. (a) Phonon dispersion curves of *Cmcm* NaC4 at 5 GPa (the magnitude of λ indicated by the thickness of the green curves). (b) Projected phonon DOS(PHDOS). (c) Eliashberg spectral function $\alpha^2F(\omega)$ (orange line), frequency-dependent EPC parameter $\lambda(\omega)$ (purple line). (d) The Fermi surface nesting function ξ_q along some q trajectories. (e) Pressure-dependence T_c , ω_{\log} , and λ of *Cmcm* NaC4.

On the other hand, the superconductivity of NaC₂ and NaC₆ is also analyzed and compared to that of NaC₄ at ambient pressure (Fig. S1, Fig. S5) [45]. The phonon vibrations between 1023 and 1487 cm⁻¹ contribute 63% to λ for NaC₂, and the part in the range of 1280-1464 cm⁻¹ contributes 64% for NaC₆. As a result, the high-frequency phonon vibrations in NaC₂ and NaC₆ play a crucial role in superconductivity, which is in sharp contrast with that of NaC₄ and CaC₆, in which low-frequency modes dominate the superconductivity [43]. The resulting λ values are 0.58 and 0.62 for NaC₂ and NaC₆, respectively, which are significantly lower than that of NaC₄. The corresponding T_c values are 13.34 K and 24.11 K for NaC₂ and NaC₆, respectively. Therefore, even though the carbon sublattice is similar in the three Na-GICs, the difference in the concentration and configuration of Na substantially modulates the EPC.

IV. Conclusions

In summary, three Na-GICs, NaC₂, NaC₄, and NaC₆, were predicted from *ab initio* evolutionary structure search. NaC₂ comprises double Na layers, NaC₄ has zigzag Na chains, and Na layers in NaC₆ feature a triangular lattice configuration. Among them, NaC₄ demonstrates a T_c of 41.2 K at 5.0 GPa, which sets a new record for reported GICs. The superconductivity of NaC₆ mainly originates from the contribution of high-

frequency phonons, which is distinct from the low-frequency ones in CaC_6 . The difference might be attributed to the stacking patterns and resulting charge transfer of C atoms. Strikingly, the predicted T_c value of NaC_2 is very close to the measured one, suggesting that the long-lasting puzzle surrounding the structure of experimental NaC_2 may have been resolved. Our findings shed light on the exploration of high- T_c superconductors in similar GICs.

Acknowledgments

This work was supported by the National Key R&D Program of China (Grant No. 2022YFA1402300), National Natural Science Foundation of China (Grants No. 52025026, No. 52090020, No. 12174200 and No. 92263101). A.R.O. acknowledges funding from the Russian Science Foundation (Grant No. 19-72-30043).

References

- [1] J. G. Bednorz and K. A. Müller, *Z. Phys. B* **64**, 189 (1986).
- [2] J. Nagamatsu, N. Nakagawa, T. Muranaka, Y. Zenitani, and J. Akimitsu, *Nature* **410**, 63 (2001).
- [3] L. Ma, K. Wang, Y. Xie, X. Yang, Y. Wang, M. Zhou, H. Liu, X. Yu, Y. Zhao, H. Wang, G. Liu, and Y. Ma, *Phys. Rev. Lett.* **128**, 167001 (2022).
- [4] N. W. Ashcroft, *Phys. Rev. Lett.* **21**, 1748 (1968).
- [5] N. W. Ashcroft, *Phys. Rev. Lett.* **92**, 187002 (2004).
- [6] P. Kong, V. S. Minkov, M. A. Kuzovnikov, A. P. Drozdov, S. P. Besedin, S. Mozaffari, L. Balicas, F. F. Balakirev, V. B. Prakapenka, S. Chariton, D. A. Knyazev, E. Greenberg, M. I. Eremets, *Nat. Commun.* **12**, 5075 (2021).
- [7] M. Somayazulu, M. Ahart, A. K. Mishra, Z. M. Geballe, M. Baldini, Y. Meng, V. V. Struzhkin, and R. J. Hemley, *Phys. Rev. Lett.* **122**, 027001 (2019).
- [8] Z. Zhang, T. Cui, M. J. Hutz, A. M. Shipley, H. Song, M. Du, V. Z. Kresin, D. Duan, C. J. Pickard, and Y. Yao, *Phys. Rev. Lett.* **128**, 047001 (2022).
- [9] X. Zhang, Y. Zhao, and G. Yang, *WIREs Comput. Mol. Sci.* **12**, e1582 (2022).
- [10] W. Chen, D. V. Semenok, X. Huang, H. Shu, X. Li, D. Duan, T. Cui, and A. R. Oganov, *Phys. Rev. Lett.* **127**, 117001 (2021).
- [11] X. Liang, A. Bergara, X. Wei, X. Song, L. Wang, R. Sun, H. Liu, R. J. Hemley, L. Wang, G. Gao, and Y. Tian, *Phys. Rev. B* **104**, 134501 (2021).
- [12] F. Lavini, M. Rejhon, and E. Riedo, *Nat. Rev. Mater.* **7**, 814 (2022).
- [13] E. D. Miller, D. C. Nesting, and J. V. Badding, *Chem. Mater.* **9**, 18 (1997).
- [14] B. Sundqvist, *Physics Reports* **909**, 1 (2021).
- [15] H. Zhou, T. Xie, T. Taniguchi, K. Watanabe, and A. F. Young, *Nature* **598**, 434 (2021).
- [16] E. A. Ekimov, V. A. Sidorov, E. D. Bauer, N. N. Mel'nik, N. J. Curro, J. D. Thompson, and S. M. Stishov, *Nature* **428**, 542 (2004).
- [17] A. Bhaumik, R. Sachan, and J. Narayan, *ACS Nano* **11**, 5351 (2017).
- [18] A. Bhaumik, R. Sachan, S. Gupta, and J. Narayan, *ACS Nano* **11**, 11915 (2017).
- [19] Y. Ge, K. Luo, Y. Liu, G. Yang, W. Hu, B. Li, G. Gao, X.-F. Zhou, B. Xu, Z. Zhao, and Y. Tian, *Mater. Today Phys.* **23**, 100630 (2022).
- [20] T. E. Weller, M. Ellerby, S. S. Saxena, R. P. Smith, and N.T. Skipper, *Nat. Phys.* **1**, 39 (2005).
- [21] N. Emery, C. Hérolde, M. d'Astuto, V. Garcia, Ch. Bellin, J. F. Marêché, P. Lagrange, and G. Loupias, *Phys. Rev. Lett.* **95**, 087003 (2005).
- [22] M. Gao, X. Kong, Z. Lu, and T. Xiang, *Acta Phys. Sin.* **64**, 214701 (2015).
- [23] A. Y. Ganin, Y. Takabayashi, Y. Z. Khimyak, S. Margadonna, A. Tamai, M. J. Rosseinsky, and K. Prassides, *Nat. Mater.* **7**, 367 (2008).
- [24] A. F. Hebard, M.J. Rosseinsky, R.C. Haddon, D.W. Murphy, S.H. Glarum, Palstra, Thomas, A.P. Ramirez, and A.R. Kortan, *Nature* **350**, 600 (1991).
- [25] M. S. Dresselhaus, G. Dresselhaus, *Adv. Phys.* **51**, 1 (2002).
- [26] I. T. Belash, O. V. Zharikov, and A. V. Palnichenko, *Synth. Met.* **34**, 47 (1990).
- [27] A. Gauzzi, S. Takashima, N. Takeshita, C. Terakura, H. Takagi, N. Emery, C. Hérolde, P. Lagrange, and G. Loupias, *Phys. Rev. Lett.* **98**, 067002 (2007).
- [28] I. T. Belash, A. D. Bronnikov, O. V. Zharikov, and A.V. Palnichenko, *Solid State Commun.* **64**, 1445 (1987).
- [29] G. Csányi, P. B. Littlewood, A. H. Nevidomskyy, C. J. Pickard and B. D. Simons, *Nat. Phys.* **1**, 42 (2005).
- [30] Q. Yang, K. Zhao, H. Liu, and S. Zhang, *J. Phys. Chem. Lett.* **12**, 5850 (2021).
- [31] A. R. Oganov and C. W. Glass, *J. Chem. Phys.* **124**, 244704 (2006).

[32] A. O. Lyakhov, A. R. Oganov, H. T. Stokes, and Q. Zhu, *Comput. Phys. Commun.* **184**, 1172 (2013)

[33] Y. Wang, J. Lv, L. Zhu, and Y. Ma, *Comput. Phys. Commun.* **183**, 2063 (2012).

[34] C. J. Pickard, and R. J. Needs, *J. Phys. Condens. Mat.* **23**, 053201 (2011).

[35] S. Goedecker, *J. Chem. Phys.* **120**, 9911 (2004).

[36] M. Amsler, and S. Goedecker, *J. Chem. Phys.* **133**, 224104 (2010).

[37] W. Kohn and L. J. Sham, *Phys. Rev.* **140**, A1133 (1965).

[38] P. Hohenberg and W. Kohn, *Phys. Rev.* **136**, B864 (1964).

[39] G. Kresse and J. Furthmüller, *Phys. Rev. B* **54**, 11169 (1996).

[40] J. P. Perdew, K. Burke, and M. Ernzerhof, *Phys. Rev. Lett.* **77**, 3865 (1996).

[41] P. E. Blöchl, *Phys. Rev. B* **50**, 17953 (1994).

[42] P. Giannozzi, S. Baroni, N. Bonini, M. Calandra, R. Car, C. Cavazzoni, D. Ceresoli, G. L. Chiarotti, M. Cococcioni, and I. Dabo, *J. Phys. Condens. Mat.* **21**, 395502 (2009).

[43] M. Calandra and F. Mauri, *Phys. Rev. Lett.* **95**, 237002 (2005).

[44] P. B. Allen, and R. C. Dynes, *Phys. Rev. B* **12**, 905 (1975).

[45] See Supplemental Material for additional electronic properties.

[46] C. H. Hu, A. R. Oganov, Q. Zhu, G. R. Qian, G. Frapper, A. O. Lyakhov, and H. Y. Zhou, *Phys. Rev. Lett.* **110**, 165504 (2013).

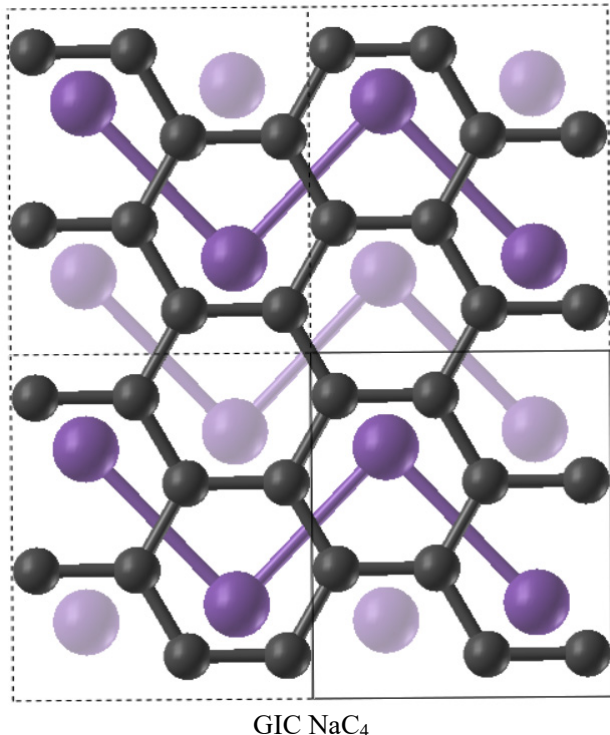
[47] N. Emery, C. Hérol, and P. Lagrange, *J. Solid State Chem.* **178**, 2947 (2005).

[48] M. F. Budyka, T. S. Zyubina, A. G. Ryabenko, S. H. Lin, and A. M. Mebel, *Chem. Phys. Lett.* **407**, 266 (2005).

[49] W. Chen, *J. Appl. Phys.* **114**, 173906 (2013).

[50] J. M. An and W. E. Pickett, *Phys. Rev. Lett.* **86**, 4366 (2001).

Table of Contents Graphic



Supplementary Materials

Superconductivity in graphite intercalation compounds with sodium

Chun-Mei Hao^{1,2}, Xing Li², Artem R. Oganov³, Jingyu Hou⁴, Shicong Ding², Yanfeng Ge², Lin Wang^{1,2},
Xiao Dong⁴, Hui-Tian Wang⁵, Guochun Yang^{2,*}, Xiang-Feng Zhou^{1,2,*}, and Yongjun Tian¹

¹*Center for High Pressure Science, State Key Laboratory of Metastable Materials Science and Technology, Yanshan University, Qinhuangdao, 066004, China*

²*Key Laboratory for Microstructural Material Physics of Hebei Province, School of Science, Yanshan University, Qinhuangdao 066004, China*

³*Skolkovo Institute of Science and Technology, Bolshoy Boulevard 30, bld. 1, Moscow 121205, Russia*

⁴*Key Laboratory of Weak-Light Nonlinear Photonics, School of Physics, Nankai University, Tianjin 300071, China*

⁵*National Laboratory of Solid State Microstructures, School of Physics, and Collaborative Innovation Center of Advanced Microstructures, Nanjing University, Nanjing 210093, China*

Email: yanggc@ysu.edu.cn; xfzhou@ysu.edu.cn

Index	Page
1. Phonon dispersion curves, projected phonon DOS (PHDOS), Eliashberg spectral function $\alpha^2F(\omega)$, and frequency-dependent EPC parameter $\lambda(\omega)$ of Na-C phases at ambient pressure.....	S3
2. Electron localization function (ELF) for Na-C phases at 5 GPa.....	S4
3. Electronic band structures and corresponding projected density of states (PDOS) of $P2_1/m$ NaC ₂ and $P6/mmm$ NaC ₆ at 5 GPa.....	S4
4. Band structure of NaC ₄ and the Fermi surface of band3 at 5 GPa.....	S5
5. The comparison of the superconductivity of $P2_1/m$ NaC ₂ , $Cmcm$ NaC ₄ , and $P6/mmm$ NaC ₆ at ambient pressure.....	S5
6. Phonon dispersion curves, projected phonon DOS(PHDOS), Eliashberg spectral function $\alpha^2F(\omega)$, and frequency-dependent EPC parameter $\lambda(\omega)$ of Na-C phases at 3.5 GPa.	S5
7. Structural information of the predicted stable Na-C phases.	S6
8. The average bond lengths of C-C in Na-C compounds compared to experimental data of graphene (1.42 Å).....	S6

Supplementary Figures

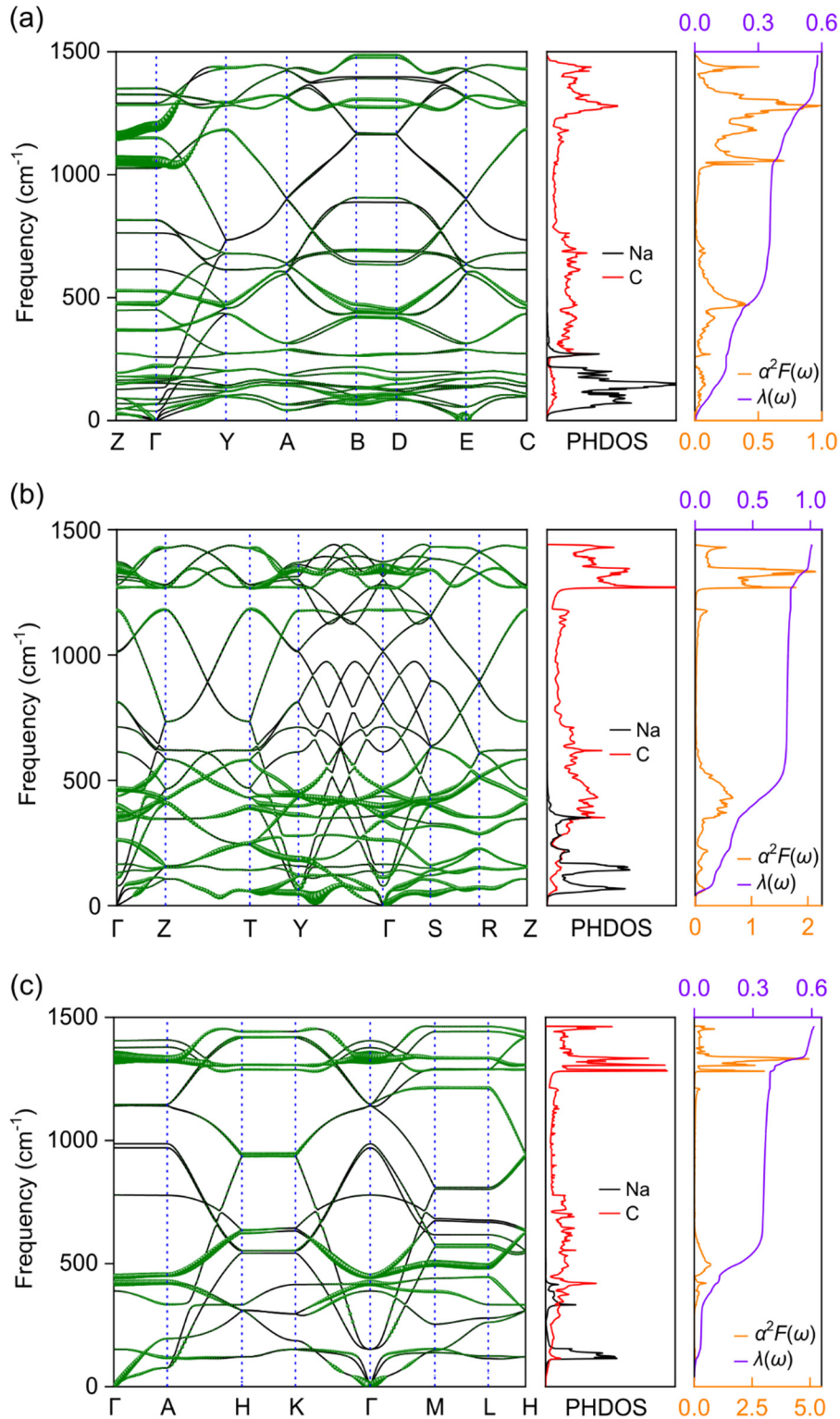


Fig. S1. Phonon dispersion curves (the magnitude of λ indicated by the thickness of the green curves), projected phonon DOS, Eliashberg spectral function $\alpha^2 F(\omega)$, and EPC parameter λ of (a) $P2_1/m$ NaC₂, (b) $Cmcm$ NaC₄, and (c) $P6/mmm$ NaC₆ at 0 GPa.

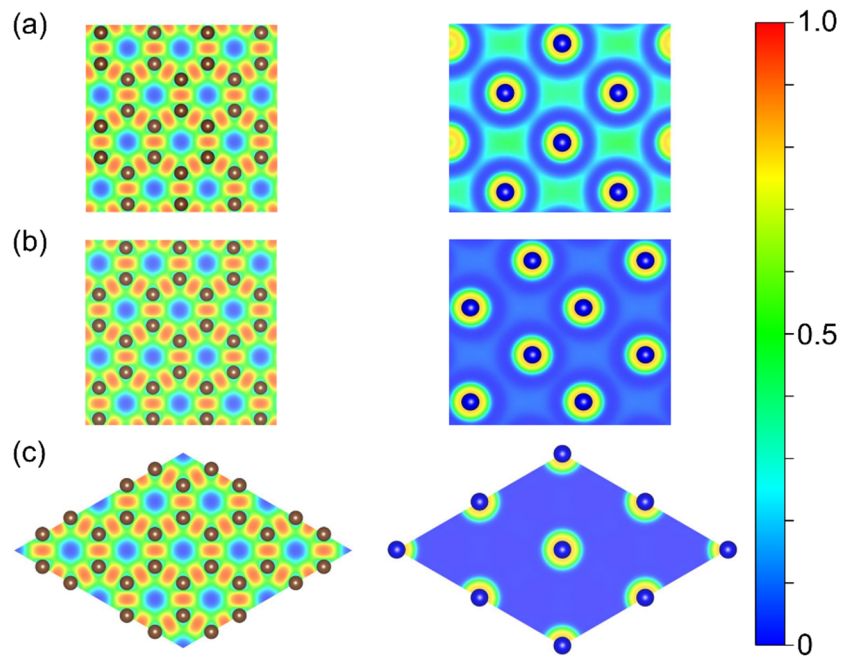


Fig. S2. Electron localization function (ELF) for (a) $P2_1/m$ NaC_2 , (b) $Cmcm$ NaC_4 , and (c) $P6/mmm$ NaC_6 at 5 GPa. The blue and brown spheres represent Na and C atoms, respectively. The left and right sides represent the ELF of graphene layer and Na layer, respectively.

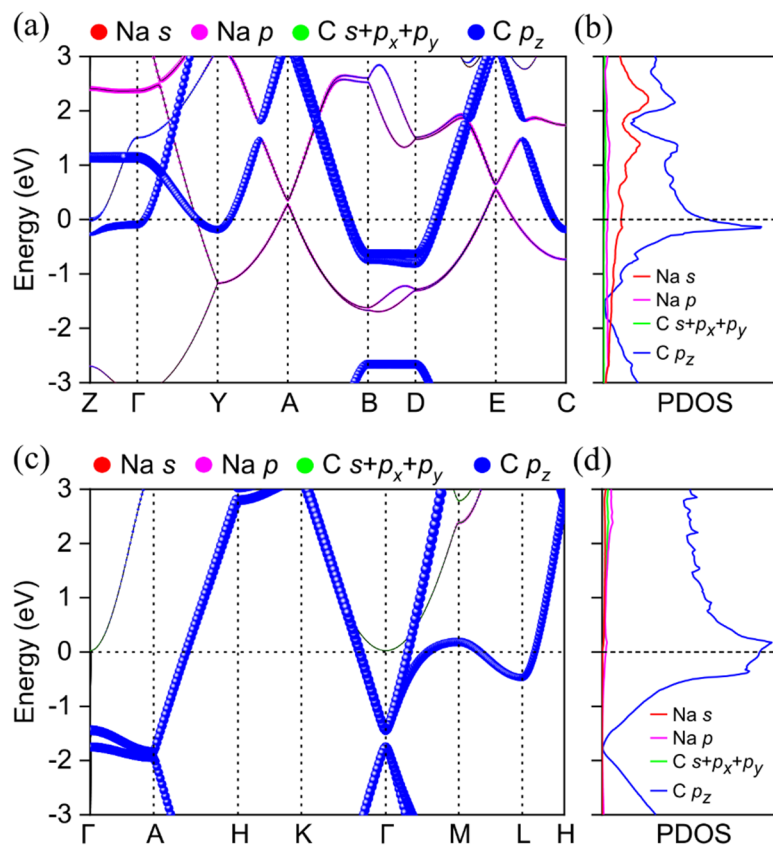


Fig. S3. (a), (b) The orbital-resolved band structures and projected density of states (PDOS) for $P2_1/m$ NaC_2 . (c), (d) for $P6/mmm$ NaC_6 at 5 GPa.

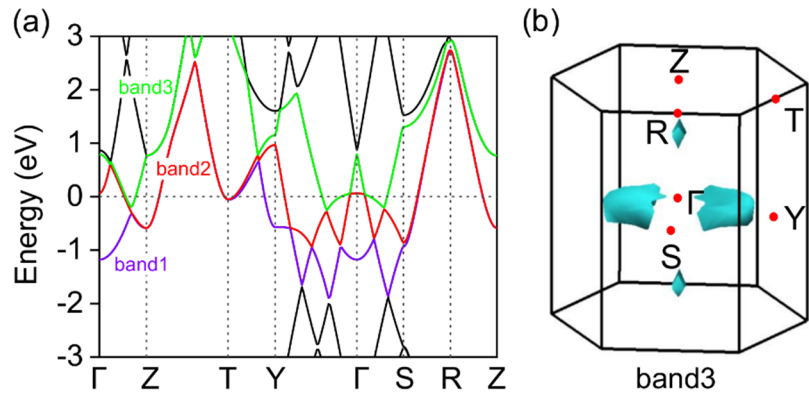


Fig. S4. (a) Band structure of $Cmcm$ NaC_4 at 5 GPa. Three bands cross the Fermi level E_F , marked as band1 (red line), band2 (purple line) and band3 (green), respectively. (b) The Fermi surface is related band3.

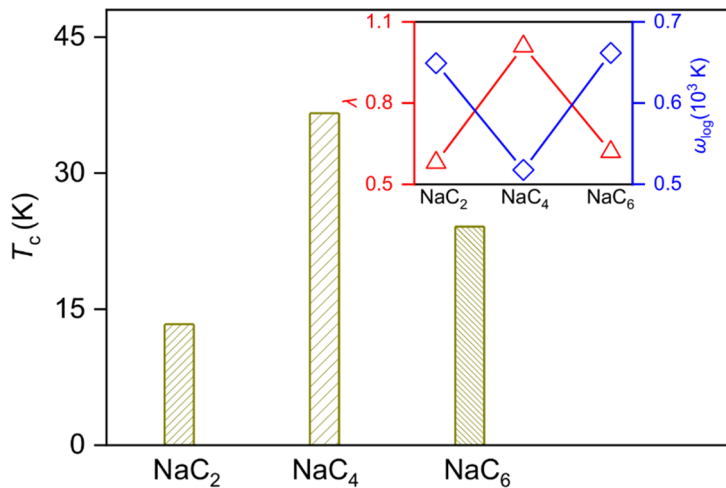


Fig. S5. The superconductivity of $P2_1/m$ NaC_2 , $Cmcm$ NaC_4 , and $P6/mmm$ NaC_6 at 0 GPa.

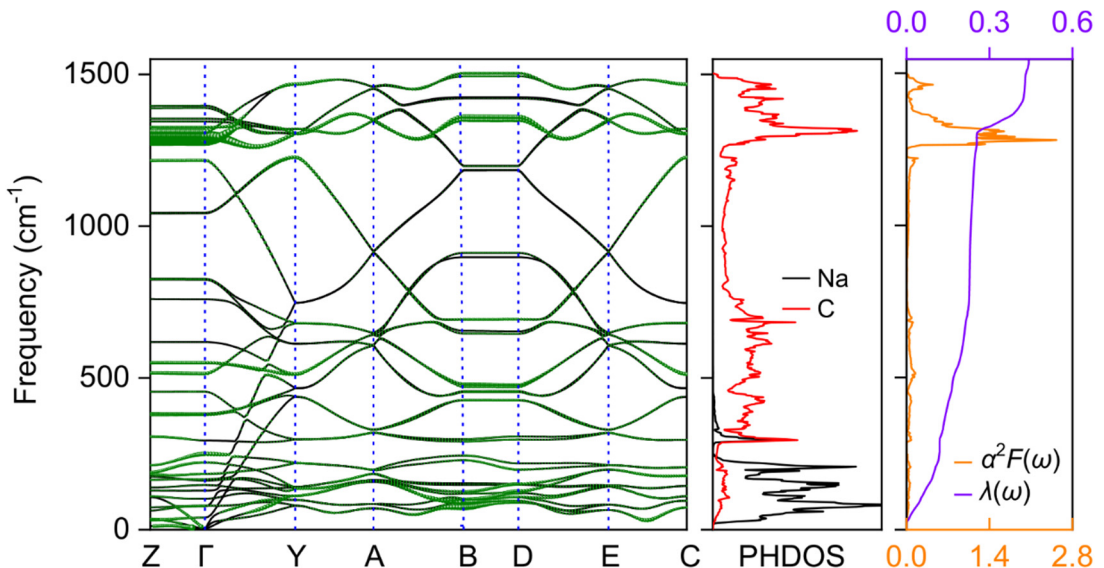


Fig. S6. Phonon dispersion curves (the magnitude of λ indicated by the thickness of the green curves), projected phonon DOS, Eliashberg spectral function $\alpha^2F(\omega)$, and EPC parameter λ of $P2_1/m$ NaC_2 at 3.5 GPa.

Supplementary Tables

Table S1. Lattice parameters and atomic positions of stable Na-C compounds at 5 GPa. It should be noted that “seeting $\bar{c}ba$ ” is performed to orient the graphene layer in NaC_4 along the c -axis.

Space group (No.)	Lattice parameters (Å)	Atomic fractional coordinates	
	$a = 4.97, b = 4.30,$	Na1 2e (0.4638, 0.7500, 0.3358)	
$P2_1/m$ - NaC_2	$c = 7.36$	Na2 2e (0.9597, 0.2500, 0.3262)	
(11)	$\alpha = \gamma = 90^\circ,$	C1 4f (0.3742, 0.9171, 0.9961)	
	$\beta = 98.68^\circ$	C2 4f (0.8751, 0.9169, 0.0006)	
$Cmcm$ - NaC_4 (63, setting $\bar{c}ba$)	$a = 4.32, b = 4.99,$ $c = 9.12$ $\alpha = \beta = \gamma = 90^\circ$	Na1 4c (-0.2500 0.2740 -0.5000) C1 16h (0.0830 -0.1251 -0.24520)	
	$a = b = 4.31$		
$P6/mmm$ - NaC_6 (191)	$c = 4.34$ $\alpha = \beta = 90^\circ,$ $\gamma = 120^\circ$	Na1 1b (0.0000 0.0000 0.5000) C1 6j (0.0000 0.3337 0.0000)	

Table S2. The average bond lengths of C-C in Na-C compounds at 5 GPa compared to experimental data of graphene (1.42 Å).

Space group	$P2_1/m$ - NaC_2	$Cmcm$ - NaC_4	$P6/mmm$ - NaC_6
Bond length (Å)	1.44	1.44	1.43